The Astrophysical Journal Letters, 902:L26 (8pp), 2020 October 10 https://doi.org/10.3847/2041-8213/abbc0a

On the Origin of GW190521-like Events from Repeated Black Hole Mergers in Star Clusters

Giacomo Fragione[1,2], Abraham Loeb[3], and Frederic A. Rasio[1,2]
[1] Center for Interdisciplinary Exploration & Research in Astrophysics (CIERA), Evanston, IL 60202, USA; giacomo.fragione90@gmail.com
[2] Department of Physics & Astronomy, Northwestern University, Evanston, IL 60202, USA
[3] Astronomy Department, Harvard University, 60 Garden Street, Cambridge, MA 02138, USA
Received 2020 September 9; revised 2020 September 25; accepted 2020 September 25; published 2020 October 13

Abstract

LIGO and Virgo have reported the detection of GW190521, from the merger of a binary black hole (BBH) with a total mass around $150\,M_{\odot}$. While current stellar models limit the mass of any black hole (BH) remnant to about 40–50 $M_{\odot}$, more massive BHs can be produced dynamically through repeated mergers in the core of a dense star cluster. The process is limited by the recoil kick (due to anisotropic emission of gravitational radiation) imparted to merger remnants, which can escape the parent cluster, thereby terminating growth. We study the role of the host cluster metallicity and escape speed in the buildup of massive BHs through repeated mergers. Almost independent of host metallicity, we find that a BBH of about $150\,M_{\odot}$ could be formed dynamically in any star cluster with escape speed $\gtrsim$200 km s^{-1}, as found in galactic nuclear star clusters as well as the most massive globular clusters and super star clusters. Using an inspiral-only waveform, we compute the detection probability for different primary masses ($\geqslant 60\,M_{\odot}$) as a function of secondary mass and find that the detection probability increases with secondary mass and decreases for larger primary mass and redshift. Future additional detections of massive BBH mergers will be of fundamental importance for understanding the growth of massive BHs through dynamics and the formation of intermediate-mass BHs.

Unified Astronomy Thesaurus concepts: Gravitational waves (678); Gravitational wave sources (677); Gravitational wave detectors (676); Gravitational wave astronomy (675); Astrophysical black holes (98); Black holes (162); Intermediate-mass black holes (816); Black hole physics (159); Globular star clusters (656); Open star clusters (1160); Star clusters (1567); Superclusters (1657)

1. Introduction

The detection of gravitational waves (GWs) has revolutionized our understanding of black holes (BHs) and neutron stars (NSs). Since the first discovery, the LIGO and Virgo observatories have confirmed the detection of more than 10 events (Aasi et al. 2015; Acernese et al. 2015; Abbott et al. 2019a, 2019b). These observations have brought several surprises, including GW190412 (The LIGO Scientific Collaboration & The Virgo Collaboration 2020a), a binary black hole (BBH) merger with a mass ratio of nearly four-to-one, GW190814 (The LIGO Scientific Collaboration & The Virgo Collaboration 2020b), a merger between a BH and a compact object of about 2.5 $M_{\odot}$, and GW190425 (The LIGO Scientific Collaboration & the Virgo Collaboration 2020c), a merger of a binary NS of total mass nearly 3.4 $M_{\odot}$, the most massive binary NS observed so far.

The origin of binary mergers is still highly uncertain, with several possible scenarios that could potentially account for most of the observed events. These include mergers from isolated evolution of binary stars (Belczynski et al. 2016; de Mink & Mandel 2016; Giacobbo & Mapelli 2018), dynamical assembly in dense star clusters (Askar et al. 2017; Banerjee 2018; Fragione & Kocsis 2018; Rodriguez et al. 2018; Samsing & Hotokezaka 2020; Hamers & Samsing 2019; Kremer et al. 2019), mergers in triple and quadruple systems induced through the Kozai–Lidov mechanism (Antonini & Perets 2012; Liu & Lai 2018; Fragione et al. 2019a, 2019b, 2020; Fragione & Kocsis 2019), and mergers of compact binaries in galactic nuclei (Bartos et al. 2017; Stone et al. 2017; Rasskazov & Kocsis 2019; McKernan et al. 2020).

Another surprise is GW190521, a BBH of total mass $\sim 150\,M_{\odot}$, consistent with the merger of two BHs with masses of $85^{+21}_{-14}\,M_{\odot}$ and $66^{+17}_{-18}\,M_{\odot}$ (The LIGO Scientific Collaboration & The Virgo Collaboration 2020d, 2020e). Current stellar models predict a dearth of BHs both with masses larger than about $50\,M_{\odot}$ (high-mass gap) and smaller than about $5\,M_{\odot}$ (low-mass gap), with exact values depending on the details of the progenitor collapse (e.g., Fryer et al. 2012). The high-mass gap results from the pulsational pair-instability process, which affects massive progenitors. Whenever the pre-explosion stellar core is in the range 45–65 $M_{\odot}$, large amounts of mass can be ejected, leaving a BH remnant with a maximum mass around 40–50 $M_{\odot}$ (Heger et al. 2003; Woosley 2017). Therefore, GW190521 challenges our understanding of massive star evolution.

BHs more massive than the limit imposed by pulsational pair-instability can be produced dynamically through repeated mergers of smaller BHs in the core of a dense star cluster, where three- and four-body interactions can catalyze the growth of a BH seed (e.g., Gültekin et al. 2004). A fundamental limit for repeated mergers comes from the recoil kick imparted to merger remnants as a result of anisotropic GW emission (Lousto et al. 2010; Lousto & Zlochower 2011). Depending on the mass ratio and the spins of the merging objects, the recoil kick can be as high as $\sim$100–1000 km s^{-1}. If it exceeds the local escape speed, the merger remnant is ejected from the system and further growth is quenched. A number of studies have shown that massive globular clusters (e.g., Rodriguez et al. 2019), super star clusters (e.g., Rodriguez et al. 2020), and nuclear clusters at the centers of galaxies (e.g., Antonini et al. 2019; Fragione & Silk 2020) are the only environments

where the mergers of second-(2g) or higher-generation (*N*g) BHs could take place.

In this Letter, we explore the possibility that GW190521-like events (BBHs with total mass around $150\,M_\odot$) are the product of repeated mergers in a star cluster. The Letter is organized as follows. In Section 2, we discuss the role of the cluster metallicity and escape speed in the assembly of massive BHs. In Section 3, we discuss the assembly of massive BHs through repeated mergers in a variety of dynamically active environments. In Section 4, we discuss the detection probability for GW190521-like events. Finally, in Section 5, we discuss the implications of our results and draw our conclusions.

2. Limits on the Hierarchical Growth of BH Seeds

Two main factors determine the ability of a BH seed to grow via repeated mergers: the environment metallicity and the host-cluster escape speed. The former sets the initial maximum seed mass, while the latter determines the maximum recoil kick that can be imparted to a merger remnant to be retained within the host cluster.

2.1. Metallicity

Dense star clusters form with a variety of initial masses, concentrations, and metallicities. Open clusters and super star clusters are high-metallicity environments (e.g., Portegies Zwart et al. 2010), in contrast to most globular clusters (e.g., Harris 1996). Nuclear star clusters present both high- and low-metallicity stars, as a result of their complex history and various episodes of accretion and star formation (e.g., Antonini 2013).

Metallicity is crucial in determining the maximum BH mass in a given environment. Low-metallicity systems can form BHs that are much more massive than high-metallicity systems. This difference is a result of stellar winds in massive stars. Higher-metallicity stars experience stronger winds and, as a consequence, larger mass-loss rates (Vink et al. 2001), resulting in less-massive BH progenitors prior to stellar collapse (Spera & Mapelli 2017). Therefore, typical globular clusters are expected to produce more massive BHs than open and super star clusters.

To demonstrate the role of metallicity, we consider a sample of stars in the mass range of BH progenitors, $[20\,M_\odot$–$150\,M_\odot]$, and evolve them using the stellar evolution code SSE (Hurley et al. 2000, 2002). We use the updated version of SSE from Banerjee et al. (2020), with the most up-to-date prescriptions for stellar winds and remnant formation; it produces remnant populations consistent with those from StarTrack (Belczynski et al. 2008). We choose four different values of the metallicity Z, namely $0.01\,Z_\odot$, $0.1\,Z_\odot$, $0.5\,Z_\odot$, and $Z_\odot$.

In Figure 1, we show the final BH mass as a function of the zero-age main-sequence (ZAMS) mass for single stars computed using SSE, for different metallicities. For solar metallicity, the maximum BH mass is of about $15\,M_\odot$, and this increases to about $35\,M_\odot$ and $45\,M_\odot$ for $Z = 0.5\,Z_\odot$ and $Z = 0.1\,Z_\odot$, respectively. Note that, for the stellar-mass range considered, metallicities lower than about $0.1\,Z_\odot$ would all produce very similar initial BH mass functions.

Metallicity, therefore, limits the initial mass of the BH seed that can undergo repeated mergers. At the same time, it also constrains the maximum mass of the BHs with which the seed can merge. In a low-metallicity cluster, GW190521 components could be 2g BHs, each the remnant of a merger of 1g BHs. On the other hand, they could be 4g or 5g BHs if their progenitors were born in a solar-metallicity environment.

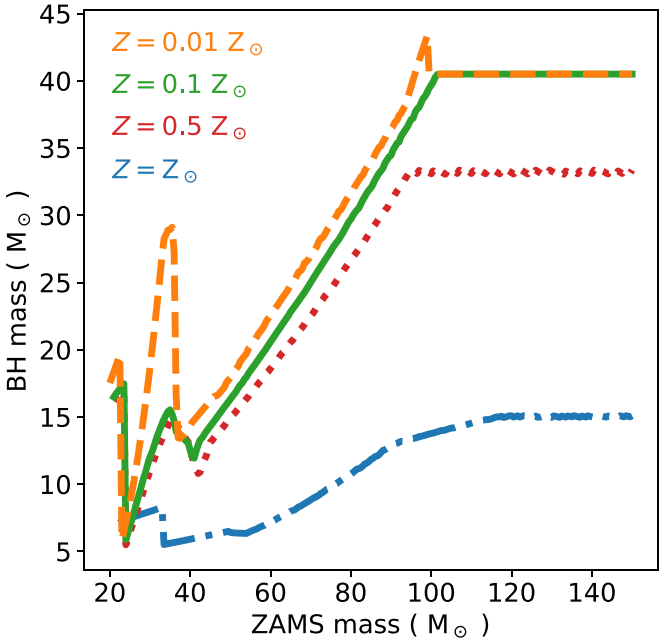

Figure 1. BH mass as a function of zero-age main-sequence (ZAMS) mass for single stars, computed using SSE (Hurley et al. 2000, 2002) with updates from Banerjee et al. (2020). The four colors denote the four different metallicities.

We note in passing that runaway growth of a very massive star could also be triggered through physical collisions if the initial density of the host cluster is sufficiently high. Such a star could eventually collapse to form a BH in the high-mass gap, or even an intermediate-mass BH (Portegies Zwart et al. 2004; Gürkan et al. 2006; Pan et al. 2012; Kremer et al. 2020). However, stellar evolution is highly unconstrained in this regime. Some models suggest that only a low-metallicity star with mass $\gtrsim 200\,M_\odot$ could directly collapse to a BH more massive than about $80\,M_\odot$ (Spera & Mapelli 2017; Renzo et al. 2020).

2.2. Recoil Kicks

The escape speed $v_{\rm esc}$ from the core of a star cluster is determined by its mass and density profile. The more massive and dense the cluster is, the higher the escape speed. Open clusters, globular clusters, and nuclear star clusters have typical escape speeds $\sim 1\,{\rm km\,s^{-1}}$, $\sim 10\,{\rm km\,s^{-1}}$, and $\sim 100\,{\rm km\,s^{-1}}$, respectively. Note, however, that the escape speed of a given environment may change over time depending on the details of its formation history and dynamical evolution (see e.g., Figure 3 Rodriguez et al. 2020).

Due to the anisotropic emission of GWs at merger, a recoil kick is imparted to the merger remnant (Lousto et al. 2012). The host escape speed then determines the fraction of retained remnants. The recoil kick depends on the asymmetric mass ratio $\eta = q/(1+q)^2$, where $q = m_2/m_1 < 1$ (m_1 and m_2 are the masses of the merging BHs), and on the magnitude of the dimensionless spins, $|\chi_1|$ and $|\chi_2|$ (corresponding to m_1 and m_2). We model the recoil kick following (Lousto et al. 2010) as

$$\mathbf{v}_{\rm kick} = v_m \hat{e}_{\perp,1} + v_\perp(\cos\xi \hat{e}_{\perp,1} + \sin\xi \hat{e}_{\perp,2}) + v_\parallel \hat{e}_\parallel, \qquad (1)$$

where

$$v_m = A\eta^2\sqrt{1-4\eta}(1+B\eta) \quad (2)$$

$$v_\perp = \frac{H\eta^2}{1+q}(\chi_{2,\parallel} - q\chi_{1,\parallel}) \quad (3)$$

$$v_\parallel = \frac{16\eta^2}{1+q}[V_{1,1} + V_A\tilde{S}_\parallel + V_B\tilde{S}_\parallel^2 + V_C\tilde{S}_\parallel^3] \times |\boldsymbol{\chi}_{2,\perp} - q\boldsymbol{\chi}_{1,\perp}|\cos(\phi_\Delta - \phi_1). \quad (4)$$

The $\perp$ and $\parallel$ refer to the directions perpendicular and parallel to the orbital angular momentum, respectively, while $\hat{e}_{\perp,1}$ and $\hat{e}_{\perp,2}$ are orthogonal unit vectors in the orbital plane. We have also defined the vector

$$\tilde{\mathbf{S}} = 2\frac{\boldsymbol{\chi}_{2,\perp} + q^2\boldsymbol{\chi}_{1,\perp}}{(1+q)^2}, \quad (5)$$

ϕ_1 as the phase angle of the binary, and ϕ_Δ as the angle between the in-plane component of the vector

$$\boldsymbol{\Delta} = M^2\frac{\boldsymbol{\chi}_2 - q\boldsymbol{\chi}_1}{1+q} \quad (6)$$

and the infall direction at merger. Finally, we adopt $A = 1.2\times10^4$ km s^{-1}, $H = 6.9\times10^3$ km s^{-1}, $B = -0.93$, $\xi = 145°$ (González et al. 2007; Lousto & Zlochower 2008), and $V_{1,1} = 3678$ km s^{-1}, $V_A = 2481$ km s^{-1}, $V_B = 1793$ km s^{-1}, $V_C = 1507$ km s^{-1} (Lousto et al. 2012). The final total spin of the merger product and its mass are computed following Rezzolla et al. (2008).

In Figure 2, we show the probability (over 10^4 realizations) to retain the merger remnant of a BBH as a function of the BBH mass ratio (q) for different cluster escape speeds: 30 km s^{-1} (top-left panel), 50 km s^{-1} (top-right panel), 100 km s^{-1} (middle-left panel), 200 km s^{-1} (middle-right panel), 300 km s^{-1} (bottom-left panel), 500 km s^{-1} (bottom-right panel). We sample BH spins from a uniform distribution in the range [0, $\chi_{\rm max}$]. The recoil kick depends crucially on the maximum intrinsic spin of the merging BHs; while for low spins $v_{\rm kick}\sim100$ km s^{-1}, for high spins $v_{\rm kick}\sim1000$ km s^{-1} (e.g., Holley-Bockelmann et al. 2008; Fragione et al. 2018a, 2020; Antonini et al. 2019; Gerosa & Berti 2019; Mapelli et al. 2020). The mass ratio also plays an important role, with the recoil kick decreasing significantly in magnitude for $q\lesssim0.1$ (both for spinning and non-spinning BHs) and for $q\gtrsim0.9$ (non-spinning BHs). Clusters with low-escape speeds ($v_{\rm esc}\lesssim100$ km s^{-1}) can only retain the merger products of very unequal-mass binaries ($q\lesssim0.1$) and the remnants of roughly equal-mass BBH mergers with low-spinning components. On the other hand, clusters with larger escape speeds ($v_{\rm esc}\gtrsim100$ km s^{-1}) can retain, with various probabilities, remnants of various mass-ratio and spins. The remnants of the merger of highly spinning equal-mass BBHs could even be ejected in very massive and dense clusters ($v_{\rm esc}\approx500$ km s^{-1}).

The host cluster escape speed plays a crucial role in the growth of a BH seed through repeated mergers. Typical small open clusters ($v_{\rm esc}\sim1$ km s^{-1}) do not provide the right environment for growth of a BH seed. If BHs are born with low spins (Fuller & Ma 2019), the recoil kick could be small enough to retain a merger product within a typical globular cluster ($v_{\rm esc}\sim10$ km s^{-1}). However, if BHs are born with high spins, only more massive and denser systems, such as nuclear star clusters ($v_{\rm esc}\sim100$ km s^{-1}), could retain the remnant. In a low-metallicity cluster, GW190521 components could be 2g BHs, remnants of the mergers of nearly equal-mass 1g BHs. To retain them in a cluster with $v_{\rm esc}\lesssim200$ km s^{-1}, the progenitors should have been born with low spins. Otherwise, the two components of GW190521 could have been formed through repeated mergers of a massive 1g BH ($\gtrsim40\,M_\odot$) with low-mass 1g BHs ($\lesssim10\,M_\odot$) in a nuclear star cluster ($v_{\rm esc}\gtrsim200$ km s^{-1}). On the other hand, in a high-metallicity environment, GW190521 components could be 4g or 5g BHs because the maximum 1g BH mass is limited to about $15\,M_\odot$. Therefore, they should be retained after several mergers. As there is a negligible probability to retain a BH remnant in the region $0.2\lesssim q\lesssim0.8$ for $v_{\rm esc}\lesssim200$ km s^{-1}, only nuclear star clusters or the most massive globular clusters and super star clusters ($v_{\rm esc}\gtrsim200$ km s^{-1}) could still form GW190521.

3. GW190521-like Events from Repeated Mergers

GW190521 is a remarkable event because both of its components are likely the remnant of a previous BBH merger (see also The LIGO Scientific Collaboration & The Virgo Collaboration 2020e). In this section, we discuss the formation of GW190521-like events, requiring that a binary of total mass $150\,M_\odot$ be formed through repeated mergers of a growing BH seed within a cluster of escape speed $v_{\rm esc}$.

We run 10^4 Monte Carlo experiments, where we simulate the growth of a BH seed via repeated mergers. After each merger, we compute the recoil kick using Equation (1). If $v_{\rm kick} > v_{\rm esc}$, we consider the BH ejected from the system and further growth is impossible; otherwise, we proceed with generating a new merger event. In our numerical experiment, the probability of forming a BBH of $150\,M_\odot$ depends mainly on four parameters:

1. the cluster metallicity Z, which fixes the maximum initial seed BH mass and the maximum mass of the BHs with which it can merge;
2. the steepness of the pairing probability for BHs in binaries that merge, $\propto(m_1+m_2)^\beta$, which sets the secondary mass;
3. the maximum spin $\chi_{\rm max}$, which affects the maximum recoil kick;
4. the escape speed from the host cluster $v_{\rm esc}$, which fixes the maximum kick velocity for the remnant to be retained within the host cluster.

In our study, we choose two values of the metallicity, $Z = Z_\odot$ and $Z = 0.01\,Z_\odot$, which fix the maximum seed mass to about $15\,M_\odot$ and $45\,M_\odot$, respectively. Note that, for the stellar-mass range considered, metallicities lower than about $0.1\,Z_\odot$ would all produce very similar initial BH mass functions (Belczynski et al. 2010). However, as mentioned above, collisions and mergers of massive stars could produce a BH remnant in the high-mass gap, or even an intermediate-mass BH (Portegies Zwart et al. 2004; Gürkan et al. 2006; Kremer et al. 2020). To explore this possibility, we also consider BH seed masses up to $100\,M_\odot$. In our models, the cluster metallicity only sets the maximum mass for the BHs with which the seed can merge. We sample the intrinsic spins at birth of BHs from a uniform distribution in the range [0, $\chi_{\rm max}$], with $0\leqslant\chi_{\rm max}\leqslant1$. We set $\beta = 4$, as appropriate for binaries formed via dynamical three-body processes (O'Leary et al. 2016). Finally we consider

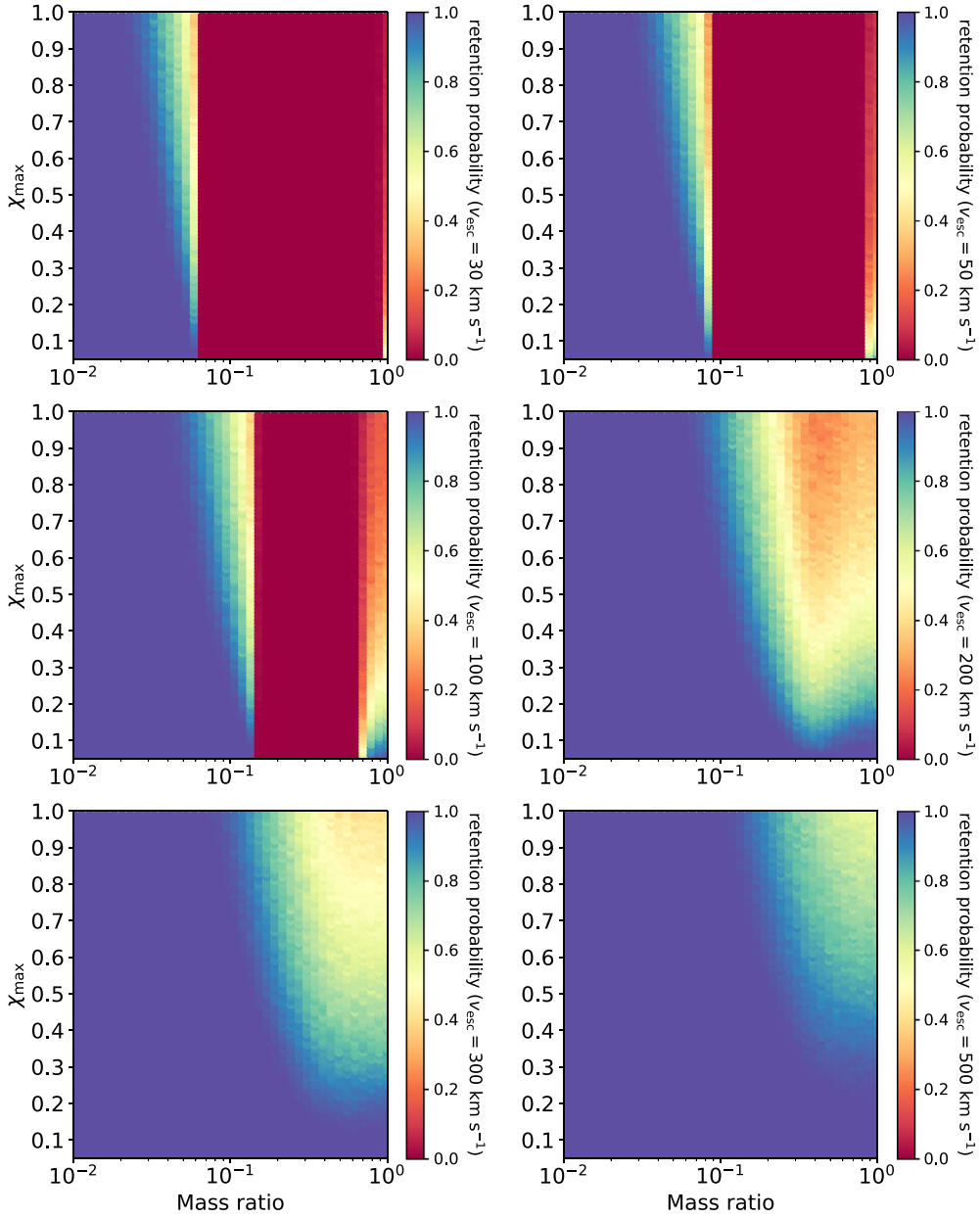

Figure 2. Probability to retain the merger remnant of a BBH as a function of the BBH mass ratio and BH spins, for different cluster escape speeds: 30 km s^{-1} (top-left panel), 50 km s^{-1} (top-right panel), 100 km s^{-1} (middle-left panel), 200 km s^{-1} (middle-right panel), 300 km s^{-1} (bottom-left panel), 500 km s^{-1} (bottom-right panel). BH spins are drawn from a uniform distribution in the range [0, $\chi_{\rm max}$].

$v_{\rm esc}$ in the range [30 km s^{-1}, 500 km s^{-1}] to encompass the full range of star clusters, from small open clusters to very massive nuclear star clusters.

Figure 3 shows the probability to form a BBH of total mass 150 $M_\odot$ as a function of the seed mass for different cluster escape speeds. We set the cluster metallicity to $Z = 0.01\,Z_\odot$. A crucial role is played by $\chi_{\rm max}$. The probability of forming a BBH of total mass of about 150 $M_\odot$ is nearly 3–4 times larger when $\chi_{\rm max} = 0.2$ than when $\chi_{\rm max} = 1$, even for clusters with large escape speeds. We find that clusters with escape speeds $\lesssim$50 km s^{-1} cannot assemble such a massive BBH because the recoil kick is too large to retain a growing BH seed, independent of the maximum spin at birth. Clusters with escape speeds of 100 km s^{-1} can form a massive BBH with total mass 150 $M_\odot$ only for large initial seed masses, $\gtrsim$70 $M_\odot$, and low spins, with $\chi_{\rm max} < 0.4$. Only star clusters with $v_{\rm esc} \gtrsim 200$ km s^{-1} could form a BBHs of 150 $M_\odot$ starting from a highly spinning BH seed of mass $\lesssim$50 $M_\odot$, which is consistent with current stellar evolutionary models for $Z = 0.01\,Z_\odot$.

In Figure 4, we explore the same parameter space but with $Z = Z_\odot$. As a general trend, solar metallicity favors the formation of a massive BBH for a wider portion of the parameter space, as the maximum BH mass is limited to 15 $M_\odot$, thus producing mostly mergers with low mass ratios. This, in turn, leads to lower recoil kicks imparted to the merger remnant, which can be retained more easily. However, if the BH seed mass is limited to 15 $M_\odot$, about the maximum mass allowed by stellar evolutionary models at solar metallicity, the formation of a BBH of about 150 $M_\odot$ is probable only for $v_{\rm esc} \gtrsim 200$ km s^{-1}.

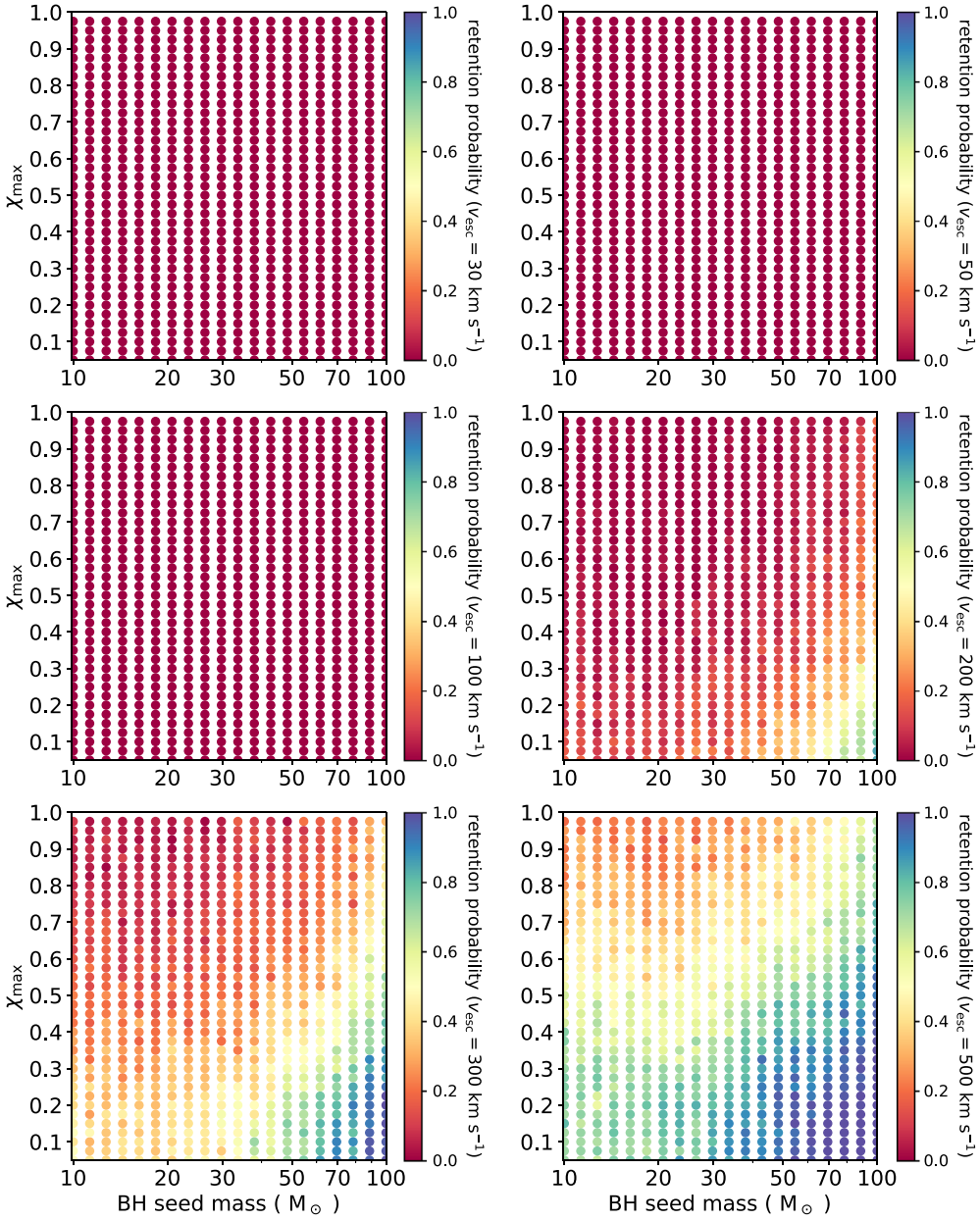

Figure 3. Probability of forming a BBH of total mass 150 $M_{\odot}$ through successive mergers as a function of the BH seed mass for different cluster escape speeds: 30 km s^{-1} (top-left panel), 50 km s^{-1} (top-right panel), 100 km s^{-1} (middle-left panel), 200 km s^{-1} (middle-right panel), 300 km s^{-1} (bottom-left panel), 500 km s^{-1} (bottom-right panel). BH spins are drawn from a uniform distribution in the range [0, $\chi_{\rm max}$]. The cluster metallicity is fixed to $Z = 0.01\ Z_{\odot}$.

We have also run models where we consider $\beta = 3$ and $\beta = 5$, to study the role of the steepness of the pairing probability for BBHs that merge. We find no significant difference from the case $\beta = 4$.

4. Detection Probability for GW190521-like Events

We now consider the probability of detecting a BBH merger where one of the components (m_1) is a massive BH.

For a source with masses m_1 and m_2, merging at a luminosity distance $D_{\rm L}$, the signal-to-noise ratio (S/N) can be expressed relative to the strain noise spectrum of a single interferometer $S_{\rm n}(f)$ and the Fourier transform $\tilde{h}(f)$ of the GW strain received at the detector by an arbitrarily oriented and located source as (O'Shaughnessy et al. 2010)

$$\rho = \sqrt{4w^2 \int_0^{f_{\rm ISCO}} \frac{|\tilde{h}(f)|^2}{S_n(f)} df}, \quad (7)$$

where w is a purely geometrical (and S/N-threshold-independent) function (see Equation (2) in O'Shaughnessy et al. 2010), which takes values between 0 and 1, and completely encompasses the detector- and source-orientation-dependent sensitivity, $f_{\rm ISCO} = c^3/(6^{1.5}\pi GM)$ is the innermost stable circular orbit (ISCO) frequency, and $|\tilde{h}(f)|$ is the frequency-domain waveform

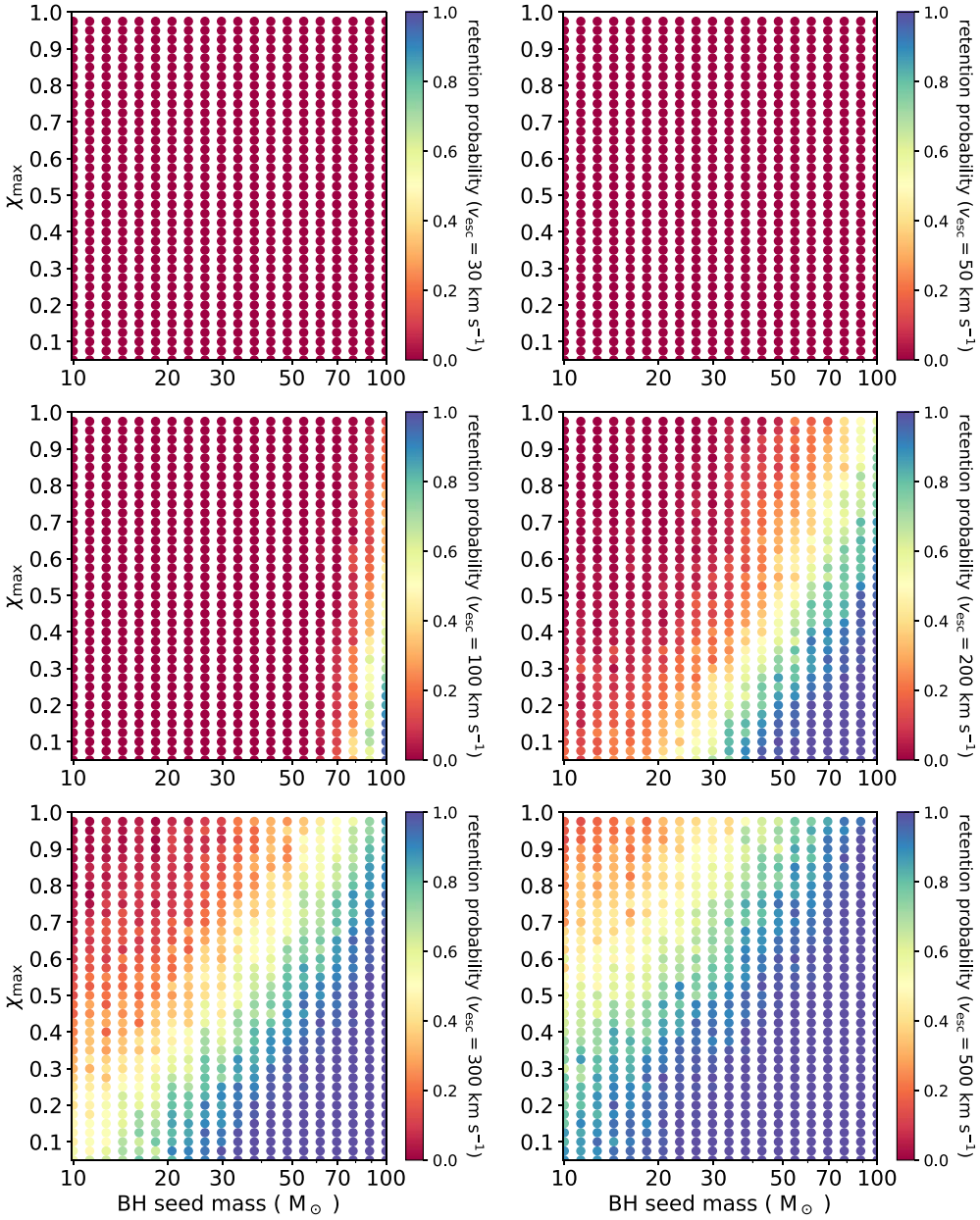

Figure 4. Same as in Figure 3, but for $Z = Z_{\odot}$.

amplitude (e.g., Equation (3) in Abadie et al. 2010)

$$|\tilde{h}(f)| = \sqrt{\frac{5}{24\pi^{4/3}}}\frac{G^{5/6}}{c^{3/2}}\frac{M_{c,z}^{5/6}}{D_L(1+z)f_{GW,z}^{7/6}}. \quad (8)$$

In the previous equation, $f_{GW,z}$ is the observed (detector frame) frequency, related to the binary orbital frequency by $f_{GW,z}(1+z) = f_{orb}$, $M_{c,z}$ is the redshifted chirp mass, related to the rest-frame chirp mass by $M_c = M_{c,z}(1+z)$, and

$$D_L = (1+z)\frac{c}{H_0}\int_0^z \frac{d\zeta}{\sqrt{\Omega_M(1+\zeta^3)+\Omega_\Lambda}}, \quad (9)$$

where z is the redshift and c and H_0 the velocity of light and Hubble constant,[4] respectively. For LIGO/Virgo we adopt a noise model from the analytical approximation of Equation (4.7) in Ajith (2011)

$$S_n(f) = 10^{-48}\,\mathrm{Hz}^{-1}(0.0152x^{-4} + 0.2935x^{9/4} + 2.7951x^{3/2} - 6.5080x^{3/4} + 17.7622), \quad (10)$$

where $x = f/245.4$ Hz, which is in excellent agreement with the publicly available Advanced LIGO design noise curve.[5]

The detection probability $p_{det}(m_1, m_2, z)$ is simply the fraction of sources of a given mass located at the given redshift that exceeds the detectability threshold in S/N, assuming that sources are uniformly distributed in sky location and orbital orientation, defined as (e.g., Dominik et al. 2015)

$$p_{det}(m_1, m_2, z) = P(\rho_{thr}/\rho_{opt}), \quad (11)$$

[4] We set $\Omega_M = 0.286$ and $\Omega_\Lambda = 0.714$ (Planck Collaboration 2016).

[5] https://dcc.ligo.org/LIGO-T0900288/public

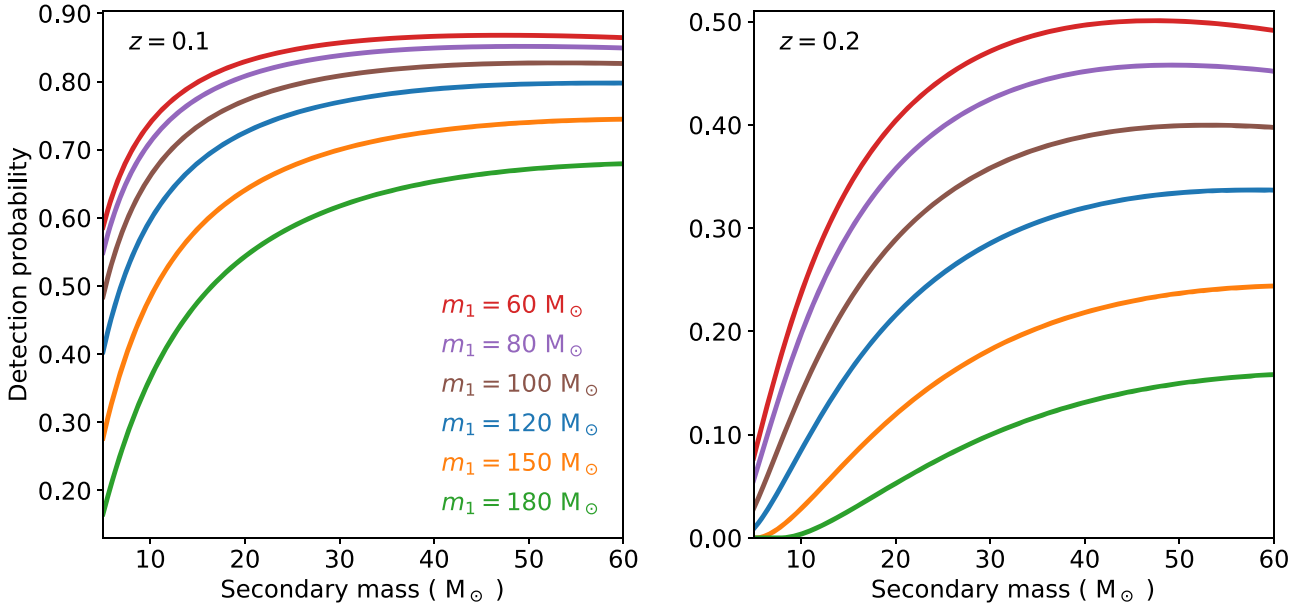

Figure 5. Detection probability (Equation (11)) for different primary masses ($\geqslant 60\,M_{\odot}$) as a function of the secondary mass, assuming an S/N threshold $\rho_{\rm thr} = 8$ and a single LIGO instrument at design sensitivity. Different colors represent different primary masses. Left panel: source redshift $z = 0.1$; right panel: source redshift $z = 0.2$.

where $\rho_{\rm opt} = \rho(w = 1)$. A good approximation is given by Equation (12) in Dominik et al. (2015)

$$P(\mathcal{W}) = a_2(1 - \mathcal{W}/\alpha)^2 + a_4(1 - \mathcal{W}/\alpha)^4 + a_8(1 - \mathcal{W}/\alpha)^8 + (1 - a_2 - a_4 - a_8)(1 - \mathcal{W}/\alpha)^{10}, \quad (12)$$

where $a_2 = 0.374222$, $a_4 = 2.04216$, $a_8 = -2.63948$, and $\alpha = 1.0$. We assume $\rho_{\rm thr} = 8$.

In Figure 5, we show the detection probability (Equation (11)) for different primary masses ($m_1 \geqslant 60\,M_{\odot}$) as a function of the secondary mass, assuming a S/N threshold $\rho_{\rm thr} = 8$ (The LIGO Scientific Collaboration & The Virgo Collaboration 2016) and a single LIGO instrument at design sensitivity (The LIGO Scientific Collaboration & The Virgo Collaboration 2018). We represent different primary masses in different colors, and fix the source redshift at $z = 0.1$ (left panel) and $z = 0.2$ (right panel). We find that the larger the secondary mass the larger the detection probability, while it decreases for larger primary masses. For $m_1 = 60\,M_{\odot}$, we find that the the detection probability is in the range 60%–90% at $z = 0.1$, which decreases to about 20%–60% for $m_1 = 180\,M_{\odot}$. As expected, a larger redshift also leads to smaller detection probabilities, which are a factor of about 2–6 smaller in the case $z = 0.2$.

Note that we have used an inspiral-only waveform and have not taken into account the S/N from merger and ringdown, which could be important for high-mass binaries, as GW190521 (see e.g., Khan et al. 2016).

5. Discussion and Conclusions

GW190521 challenges our current understanding of stellar evolution for massive stars. Stellar models predict that whenever the pre-collapse stellar core is approximately in the range $45\,M_{\odot}$–$65\,M_{\odot}$, large amounts of mass can be ejected following the onset of the pulsational pair-instability process, leaving a BH remnant with a maximum mass around $40\,M_{\odot}$–$50\,M_{\odot}$ (Woosley 2017). As only a rare star of extremely low-metallicity and mass $\gtrsim 200\,M_{\odot}$ could collapse to a BH of mass $\gtrsim 80\,M_{\odot}$ (Spera & Mapelli 2017; Renzo et al. 2020), GW190521 is unlikely to have been born as an isolated binary.

BHs more massive than the limit imposed by pulsational pair-instability could be produced dynamically through repeated mergers of smaller BHs in the core of a dense star cluster. However, the recoil kick imparted to the merger remnant, which crucially depends on the BBH mass ratio and the distribution of BH spins at birth, could eject it out of the parent cluster, terminating growth (Antonini et al. 2019; Fragione & Silk 2020).

We have simulated the growth of massive BHs starting from different BH seeds, as a function of the maximum BH spin, $\chi_{\rm max}$, in host star clusters with various metallicities and escape speeds. We have found that the probability of forming GW190521-like events with total mass around $150\,M_{\odot}$ depends crucially on the maximum BH spin at birth. The probability of forming such massive BBHs is about 3 times larger with $\chi_{\rm max} = 0.2$ than with $\chi_{\rm max} = 1$, even for clusters with large escape speeds. Almost independent of metallicity, we have demonstrated that only nuclear star clusters or the most massive globular clusters and super star clusters could form BBHs with total mass around $150\,M_{\odot}$. This conclusion does not change when higher-mass seeds ($\gtrsim 50\,M_{\odot}$) are considered.

If GW190521 was formed in a low-metallicity cluster, such as an old globular cluster, its components could be 2g BHs, remnants of previous mergers of nearly equal-mass 1g BHs. We have shown that in a cluster with $v_{\rm esc} \lesssim 200\,{\rm km\,s^{-1}}$, the progenitor 1g BHs must then have been born with low spins. Otherwise, the two components of GW190521 could have been formed through repeated minor mergers of a massive 1g BH with low-mass 1g BHs ($\lesssim 10\,M_{\odot}$) in a nuclear star cluster ($v_{\rm esc} \gtrsim 200\,{\rm km\,s^{-1}}$). On the other hand, if GW190521 was born in a high-metallicity environment, its components could be 4g or 5g BHs, which have to be retained after several mergers. Because there is a negligible probability of retaining a remnant for $0.2 \lesssim q \lesssim 0.8$ for $v_{\rm esc} \lesssim 200\,{\rm km\,s^{-1}}$, we have demonstrated that only a nuclear star cluster or the most massive globular clusters and super star clusters (with $v_{\rm esc} \gtrsim 200\,{\rm km\,s^{-1}}$) could form GW190521.

We have also computed the detection probability for different primary masses ($\geqslant 60\,M_{\odot}$) as a function of the secondary mass, assuming an S/N threshold $\rho_{\rm thr}=8$ (The LIGO Scientific Collaboration & The Virgo Collaboration 2016) and a single LIGO instrument at design sensitivity (The LIGO Scientific Collaboration & The Virgo Collaboration 2018). We have found that the larger the secondary mass is, the larger the detection probability becomes. On the other hand the detection probability decreases for larger primary masses and redshifts.

GW190521 is a remarkable event that challenges our current theoretical understanding of BBH formation, opening debates about its origin and detection (e.g., De Luca et al. 2020; Fishbach & Holz 2020; Gayathri et al. 2020; Liu & Bromm 2020; Liu & Lai 2020; Rice & Zhang 2020; Romero-Shaw et al. 2020; Palmese & Conselice 2020; Safarzadeh & Haiman 2020; Sakstein et al. 2020; Samsing & Hotokezaka 2020). Future detections of such massive mergers will help constrain our models for the growth of massive BHs through stellar dynamics and the formation of intermediate-mass BHs (Fragione et al. 2018a, 2018b; Fragione & Bromberg 2019; Greene et al. 2019).

G.F. acknowledges support from a CIERA Fellowship at Northwestern University. F.A.R. acknowledges support from NSF Grant AST-1716762. This work was supported in part by Harvard's black hole Initiative, which is funded by grants from JFT and GBMF.

ORCID iDs

Giacomo Fragione https://orcid.org/0000-0002-7330-027X
Abraham Loeb https://orcid.org/0000-0003-4330-287X
Frederic A. Rasio https://orcid.org/0000-0002-7132-418X

References

Aasi, J., Abbott, B. P., Abbott, R., et al. 2015, CQGra, 32, 074001
Abadie, J., Abbott, B. P., Abbott, R., et al. 2010, CQGra, 27, 173001
Abbott, B. P., Abbott, R., Abbott, T. D., et al. 2019a, ApJL, 882, L24
Abbott, B. P., Abbott, R., Abbott, T. D., et al. 2019b, PRX, 9, 031040
Acernese, F., Agathos, M., Agatsuma, K., et al. 2015, CQGra, 32, 024001
Ajith, P. 2011, PhRvD, 84, 084037
Antonini, F. 2013, ApJ, 763, 62
Antonini, F., Gieles, M., & Gualandris, A. 2019, MNRAS, 486, 5008
Antonini, F., & Perets, H. B. 2012, ApJ, 757, 27
Askar, A., Szkudlarek, M., Gondek-Rosińska, D., Giersz, M., & Bulik, T. 2017, MNRAS, 464, L36
Banerjee, S. 2018, MNRAS, 473, 909
Banerjee, S., Belczynski, K., Fryer, C. L., et al. 2020, A&A, 639, A41
Bartos, I., Kocsis, B., Haiman, Z., & Márka, S. 2017, ApJ, 835, 165
Belczynski, K., Dominik, M., Bulik, T., et al. 2010, ApJL, 715, L138
Belczynski, K., Kalogera, V., Rasio, F. A., et al. 2008, ApJS, 174, 223
Belczynski, K., Repetto, S., Holz, D. E., et al. 2016, ApJ, 819, 108
De Luca, V., Desjacques, V., Franciolini, G., Pani, P., & Riotto, A. 2020, arXiv:2009.01728
de Mink, S. E., & Mandel, I. 2016, MNRAS, 460, 3545
Dominik, M., Berti, E., O'Shaughnessy, R., et al. 2015, ApJ, 806, 263
Fishbach, M., & Holz, D. E. 2020, arXiv:2009.05472
Fragione, G., & Bromberg, O. 2019, MNRAS, 488, 4370
Fragione, G., Ginsburg, I., & Kocsis, B. 2018a, ApJ, 856, 92
Fragione, G., Grishin, E., Leigh, N. W. C., Perets, H. B., & Perna, R. 2019a, MNRAS, 488, 47
Fragione, G., & Kocsis, B. 2018, PhRvL, 121, 161103
Fragione, G., & Kocsis, B. 2019, MNRAS, 486, 4781
Fragione, G., Leigh, N. W. C., Ginsburg, I., & Kocsis, B. 2018b, ApJ, 867, 119
Fragione, G., Leigh, N. W. C., & Perna, R. 2019b, MNRAS, 488, 2825
Fragione, G., Loeb, A., & Rasio, F. A. 2020, ApJL, 895, L15
Fragione, G., & Silk, J. 2020, MNRAS, 498, 4591
Fryer, C. L., Belczynski, K., Wiktorowicz, G., et al. 2012, ApJ, 749, 91
Fuller, J., & Ma, L. 2019, ApJL, 881, L1
Gayathri, V., Healy, J., Lange, J., et al. 2020, arXiv:2009.05461
Gerosa, D., & Berti, E. 2019, PhRvD, 100, 041301
Giacobbo, N., & Mapelli, M. 2018, MNRAS, 480, 2011
González, J. A., Sperhake, U., Brügmann, B., Hannam, M., & Husa, S. 2007, PhRvL, 98, 091101
Greene, J. E., Strader, J., & Ho, L. C. 2019, arXiv:1911.09678
Gültekin, K., Miller, M. C., & Hamilton, D. P. 2004, ApJ, 616, 221
Gürkan, M. A., Fregeau, J. M., & Rasio, F. A. 2006, ApJL, 640, L39
Hamers, A. S., & Samsing, J. 2019, MNRAS, 487, 5630
Harris, W. E. 1996, AJ, 112, 1487
Heger, A., Fryer, C. L., Woosley, S. E., Langer, N., & Hartmann, D. H. 2003, ApJ, 591, 288
Holley-Bockelmann, K., Gültekin, K., Shoemaker, D., & Yunes, N. 2008, ApJ, 686, 829
Hurley, J. R., Pols, O. R., & Tout, C. A. 2000, MNRAS, 315, 543
Hurley, J. R., Tout, C. A., & Pols, O. R. 2002, MNRAS, 329, 897
Khan, S., Husa, S., Hannam, M., et al. 2016, PhRvD, 93, 044007
Kremer, K., Rodriguez, C. L., Amaro-Seoane, P., et al. 2019, PhRvD, 99, 063003
Kremer, K., Spera, M., Becker, D., et al. 2020, arXiv:2006.10771
Liu, B., & Bromm, V. 2020, arXiv:2009.11447
Liu, B., & Lai, D. 2018, ApJ, 863, 68
Liu, B., & Lai, D. 2020, arXiv:2009.10068
Lousto, C. O., Campanelli, M., Zlochower, Y., & Nakano, H. 2010, CQGra, 27, 114006
Lousto, C. O., & Zlochower, Y. 2008, PhRvD, 77, 044028
Lousto, C. O., & Zlochower, Y. 2011, PhRvL, 107, 231102
Lousto, C. O., Zlochower, Y., Dotti, M., & Volonteri, M. 2012, PhRvD, 85, 084015
Mapelli, M., Santoliquido, F., Bouffanais, Y., et al. 2020, arXiv:2007.15022
McKernan, B., Ford, K. E. S., & O'Shaughnessy, R. 2020, arXiv:2002.00046
O'Leary, R. M., Meiron, Y., & Kocsis, B. 2016, ApJL, 824, L12
O'Shaughnessy, R., Kalogera, V., & Belczynski, K. 2010, ApJ, 716, 615
Palmese, A., & Conselice, C. J. 2020, arXiv:2009.10688
Pan, T., Loeb, A., & Kasen, D. 2012, MNRAS, 423, 2203
Planck Collaboration 2016, A&A, 594, A13
Portegies Zwart, S. F., Baumgardt, H., Hut, P., Makino, J., & McMillan, S. L. W. 2004, Natur, 428, 724
Portegies Zwart, S. F., McMillan, S. L. W., & Gieles, M. 2010, ARA&A, 48, 431
Rasskazov, A., & Kocsis, B. 2019, ApJ, 881, 20
Renzo, M., Farmer, R., Justham, S., et al. 2020, A&A, 640, A56
Rezzolla, L., Barausse, E., Dorband, E. N., et al. 2008, PhRvD, 78, 044002
Rice, J. R., & Zhang, B. 2020, arXiv:2009.11326
Rodriguez, C. L., Amaro-Seoane, P., Chatterjee, S., & Rasio, F. A. 2018, PhRvL, 120, 151101
Rodriguez, C. L., Kremer, K., Grudić, M. Y., et al. 2020, ApJL, 896, L10
Rodriguez, C. L., Zevin, M., Amaro-Seoane, P., et al. 2019, PhRvD, 100, 043027
Romero-Shaw, I. M., Lasky, P. D., Thrane, E., & Calderon Bustillo, J. 2020, arXiv:2009.04771
Safarzadeh, M., & Haiman, Z. 2020, arXiv:2009.09320
Sakstein, J., Croon, D., McDermott, S. D., Straight, M. C., & Baxter, E. J. 2020, arXiv:2009.01213
Samsing, J., & Hotokezaka, K. 2020, arXiv:2006.09744
Spera, M., & Mapelli, M. 2017, MNRAS, 470, 4739
Stone, N. C., Metzger, B. D., & Haiman, Z. 2017, MNRAS, 464, 946
The LIGO Scientific Collaboration, & the Virgo Collaboration 2016, ApJL, 833, L1
The LIGO Scientific Collaboration, & The Virgo Collaboration 2018, LRR, 21, 3
The LIGO Scientific Collaboration, & The Virgo Collaboration 2020a, arXiv:2004.08342
The LIGO Scientific Collaboration, & The Virgo Collaboration 2020b, ApJL, 896, L44
The LIGO Scientific Collaboration, & The Virgo Collaboration 2020c, ApJL, 892, L3
The LIGO Scientific Collaboration, & The Virgo Collaboration 2020d, arXiv:2009.01075
The LIGO Scientific Collaboration, & The Virgo Collaboration 2020e, ApJL, 900, L13
Vink, J. S., de Koter, A., & Lamers, H. J. G. L. M. 2001, A&A, 369, 574
Woosley, S. E. 2017, ApJ, 836, 244